MOEM

Modern Electronic Materials 2021; 7(4): 167–175
DOI 10.3897/j.moem.7.4.78569

Research Article

Effect of contact phenomena on the electrical conductivity of reduced lithium niobate

Andrey S. Shportenko[1], Alexander M. Kislyuk[1], Andrei V. Turutin[1], Ilya V. Kubasov[1], Mikhail D. Malinkovich[1], Yuri N. Parkhomenko[1,2]

1 National University of Science and Technology MISiS, 4 Leninsky Ave., Moscow 119049, Russia

2 Federal State Research and Develpment Institute of Rare Metal Industry (Giredmet JSC), Elektrodnaya Str., Moscow 111524, Russia

Corresponding author: Andrey S. Shportenko (kapmah666@yandex.com)

Received 28 November 2021 ♦ **Accepted** 17 December 2021 ♦ **Published** 30 December 2021

Citation: Shportenko AS, Kislyuk AM, Turutin AV, Kubasov IV, Malinkovich MD, Parkhomenko YuN (2021) Effect of contact phenomena on the electrical conductivity of reduced lithium niobate. *Modern Electronic Materials* 7(4): 167–175. https://doi.org/10.3897/j.moem.7.4.78569

Abstract

Lithium niobate is a ferroelectric material finding a wide range of applications in optical and acoustic engineering. Annealing of lithium niobate crystals in an oxygen-free environment leads to appearance of black coloration and concomitant increasing electrical conductivity due to chemical reduction. There are plenty of literary data on the electrophysical properties of reduced lithium niobate crystals though contact phenomena occurring during electrical conductivity measurement as well as issues of interaction between the electrode material and the test specimens are almost disregarded. The effect of chromium and indium tin oxide electrodes on the results of measurements of electrophysical parameters at room temperature for lithium niobate specimens reduced at 1100 °C has been investigated. It was found that significant nonlinearities in the VACs of the specimens at below 5 V distort the specific resistivity readings for lithium niobate. This requires measurements at higher voltages. Impedance spectroscopy studies have shown that the measurement results are largely affected by capacities including those probably induced near the contacts. It has been shown that the experimental results are described adequately well by a model implying the presence of near-contact capacities that are parallel to the specimen's own capacity. Possible mechanism of the induction of these capacities has been described and a hypothesis has been proposed of the high density of electron states at the electrode/specimen interface that can trap carriers, the concentration of trapped carriers growing with an increase in annealing duration.

Keywords

ferroelectric, lithium niobate, monodomain crystal, reduction annealing, electrical conductivity, contact phenomena, chromium, indium tin oxide, impedance.

1. Introduction

Lithium niobate ($LiNbO_3$) is a ferroelectric oxide finding multiple applications in quantum optics, acousto- and optoelectronics engineering. Lithium niobate is used for the fabrication of surface acoustic wave delay lines and electrooptical laser radiation modulators and is a promising material for device applications, e.g. vibration sensors, dump energy collectors, actuators, magnetoelectric sensors and charged domain wall devices [1–4].

Most applications based on the electrical properties of lithium niobate require the possibility of controlling the electrical parameters of the material. For example lithium niobate based devices for operation at variable

temperature face a big problem of parasitic pyroelectric currents [5, 6] which can be reduced by increasing the electrical conductivity of the material. Charge transfer in lithium niobate single crystals is commonly described by two electrical conductivity models [7]. At high temperatures (above 450 °C) the electrical conductivity is brought about by intrinsic carriers [8]. At low temperatures the main contribution to lithium niobate conductivity is believed to be from defects and the related conductivity mechanisms. One method of changing the conductivity of lithium niobate crystals is annealing in an oxygen–free atmosphere [9, 10] which triggers oxygen and lithium diffusion. Part of the diffusion-generated lithium vacancies are filled by niobium atoms causing the formation of antisite defects which may form small-radius polarons when exposed to an electron field. It is believed that these carriers deliver the main contribution to the low-temperature conductivity of lithium niobate crystals (below ~400 °C [8]) after annealing in an oxygen–free atmosphere [11, 12].

Despite the plenty literary data on the effect of reduction heat treatment parameters on the electrophysical properties of lithium niobate, the effect of contact material on experimental results has been studied insufficiently yet. Most of earlier works did not justify the choice of contact material, this complicating comparison between results obtained by different research teams. Table 1 shows the main parameters of electrodes used for lithium niobate measurements in earlier works [5, 6, 8, 9, 12, 14–20].

Below we analyze the effect of electrode material on the constant current volt-ampere characteristics of lithium niobate and room temperature electrophysical parameters as a function of frequency. These studies deliver data on the ohmicity of the contacts, specific resistivity of the specimen material and presence or absence of ionic currents through the specimen.

2. Experimental

The specimens were made from a *z*-cut 0.5 mm thick lithium niobate wafer produced by Roditi International Corp. Ltd., UK, of congruent composition. The wafer was cut into rectangular specimens 15 × 7 mm^2 in size. The specimens were vacuum annealed at a residual gas pressure of within 10^{-6} Torr (1 Torr ≈ 133.322 Pa) at 1050 °C for 2, 20 and 40 min. in a reactive furnace in a cell made of sapphire screens separated from the specimen by polycor spacers (VK-100 vacuum tight aluminum oxide ceramic). The specimens were placed on rails of the same material as the specimens (lithium niobate) for preventing diffusion of impurity atoms from the tackle. Schematic of the cell is shown in Fig. 1.

Table 1. Electrodes used for study of lithium niobate electrophysical parameters

Parameter tested	Electrodes used	Ref.
Optical properties and electrical conductivity of reduced lithium niobate at different temperatures	Conductive rubber	[13]
Surface coustic wave devices based on reduced lithium niobate	Aluminum / titanium sputtering	[6]
Electrical conductivity as a function of reduction temperature	–	[5, 9, 14]
Electrical conductivity as a function of reduction mode	Aluminum electrodes	[15]
Piezoelectric parameters and electrical conductivity of reduced lithium niobate	Platinum electrodes	[8]
Electrical conductivity of domain boundary in lithium niobate	Chromium / gold electrodes	[16]
High-temperature electrical conductivity of nonstiochiometric lithium niobate	Platinum electrodes	[12]
Electrical conductivity and pyroelectric properties of lithium niobate	Indium and aluminum electrodes	[17]
Electrical conductivity of lithium niobate and lithium tantalate	Chromium electrodes	[18]
Frequency dependences of dielectric permeability and dielectric loss tangent of lithium niobate	Silver paste electrodes	[19]

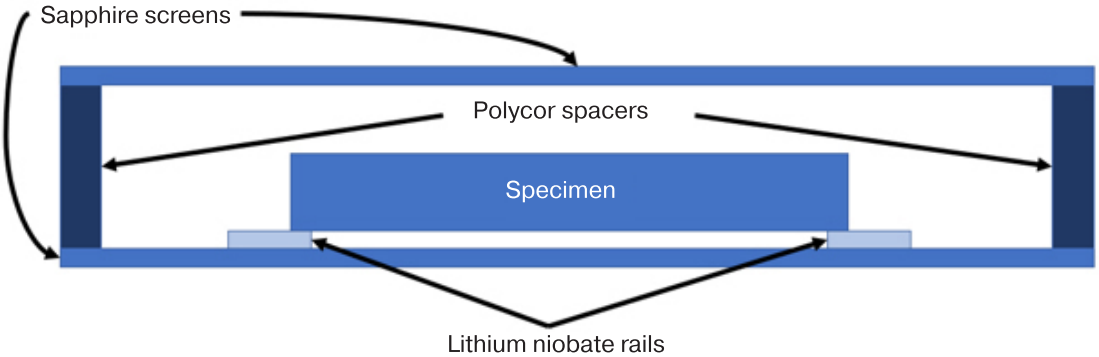

Figure 1. Schematic of cell for reduction annealing of lithium niobate.

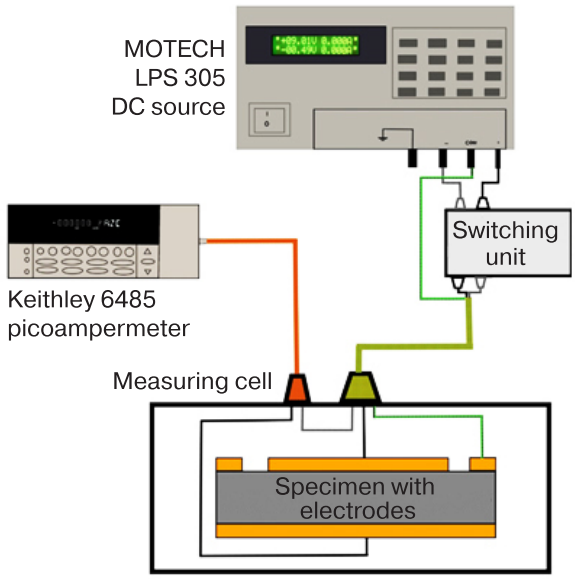

Figure 2. Schematic of DC VAC measurement experimental setup.

The as-annealed specimens were cut into 7 × 7 mm^2 squares onto which indium lead oxide and chromium (Cr) electrodes were deposited by magnetron sputtering through a mask. The as-deposited films might contain up to 10 at.% oxygen (for Cr) and up to 4 at.% nitrogen. The specimens were placed into a holder that minimized mechanical impact (soft pressure contacts).

The constant current electrical conductivity was measured on an experimental set consisting of a (MOTECH LPS 305 DC source, a Keithley 6485 picoampermeter, a switching unit and a measuring cell in the form of a screened box in which the holder with the specimen was placed. Schematic of the experimental setup is shown in Fig. 2

The electrical conductivity was measured in two stages with different voltage amplitudes and measurement steps (Fig. 3). Each stage included three measurement cycles for each of which the voltage was measured stepwise with a 0.1 V step from zero to an amplitude of ±5 V for the first stage and with a 1 V step from zero to an amplitude of ±25 V for the second stage. The cycle duration was approx. 6 h. This measurement setup yielded the volt-ampere curves **(VAC)** of the specimens with sufficient voltage stepping for low (±5 V) and high (±25 V) voltage amplitudes with minimum time consumption.

It was reported earlier [18] that recording of VACs for oxide crystals can be affected by relaxation processes manifested as a decrease in the current through the specimen in time at a constant applied bias. The relaxation processes were attributed to polarization and polarization currents [18]. Current as a function of time for each DC voltage value was measured in order to evaluate potential relaxation processes during VAC recording for the test specimens. The electrical resistivities R were calculated from the slope of rectilinear VAC sections and the specific resistivities were calculated taking into account the specimen dimensions. The frequency impedance curves were measured using a Zurich MFLI lock-in amplifier. The results were presented in the form of Nyquist diagrams. The voltage amplitude for the impedance measurements was 300 mV. Charge transfer through the specimens was simulated using equivalent circuits as shown in Fig. 4.

The equivalent circuit shown in Fig. 4 *a* is a perfect case of charge transfer through a specimen with perfect Ohmic contacts. For the calculation of this circuit the specimen's resistive component R_{VAC} was accepted to be the resistivity obtained from the VAC measurements. The C_{geom} parameter was calculated as the capacity of a flat capacitance the dielectric permeability of which is equal to that of the specimen. The impedance calculation formula is as follows:

$$Z = \frac{1}{\left(\frac{1}{R} + 2\pi i f C\right)},$$

where i is the imaginary unit and f is the applied bias frequency.

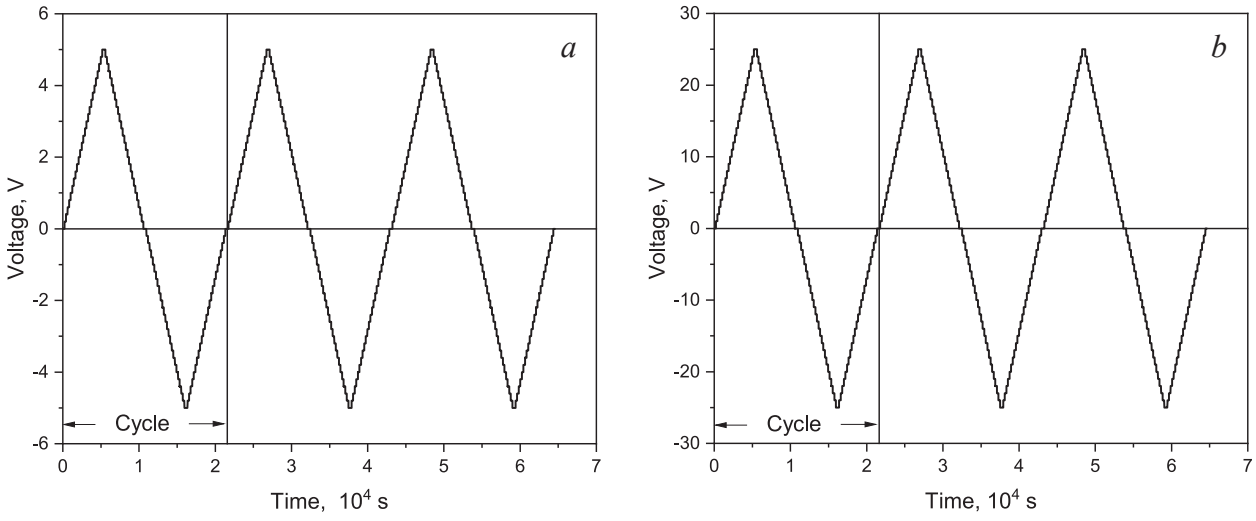

Figure 3. Applied bias as a function of time for voltage amplitudes of (*a*) 5 and (*b*) 25 V.

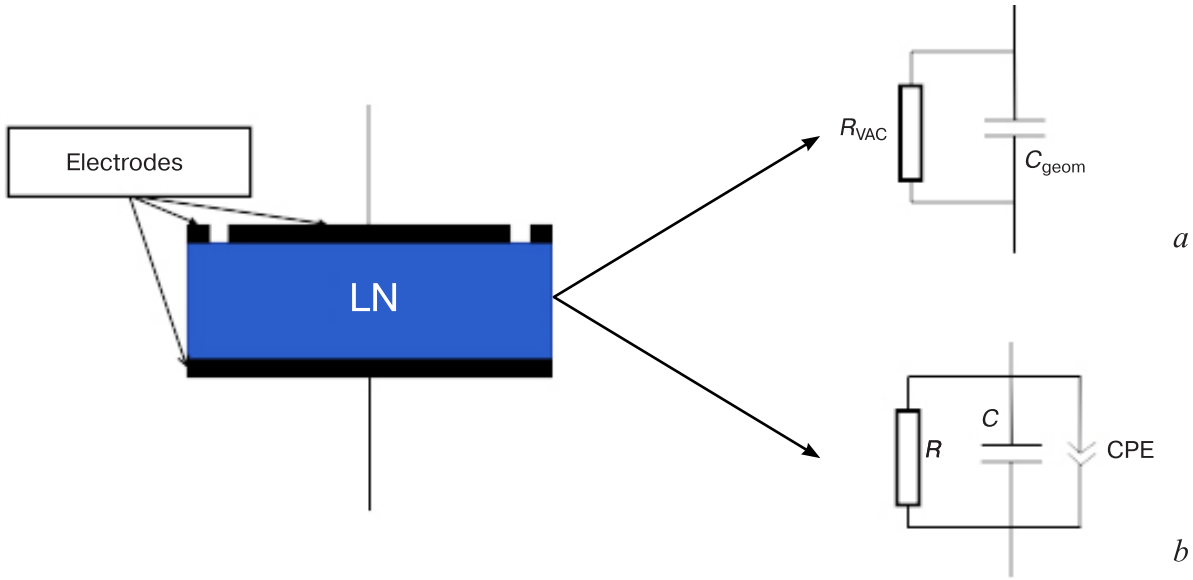

Figure 4. Schematic of specimens with electrodes and equivalent circuits used for impedance spectroscopy data approximation.

The equivalent circuit shown in Fig. 4 *b* is a system in which an additional constant phase element **(CPE)** forms in the near-electrode region of the specimen. All the other parameters are the same as for the equivalent circuit shown in Fig. 4 *b*. The overall capacity is the sum of the capacities of the specimen and the near-contact region which is simulated by the CPE element. Then the overall impedance calculation formula takes on as follows:

$$Z = \frac{1}{\left(\frac{1}{R} + 2\pi i f C + (2\pi i f)^n CPE\right)}, \quad (1)$$

where n is the exponent describing the phase shift of the variable component of the signal at the lithium niobate / contact interface.

The resistivity of the electrodes and the measuring wiring was neglected since this figure is more than two orders of magnitude smaller than R and R_{VAC}.

Capacities related to specimen areas and specific resistivities ρ_{imp} were calculated from the electrical capacity and resistivity of the specimens measured by impedance spectroscopy taking into account specimen dimensions.

3. Results and discussion

3.1. Volt-ampere curve measurement

Figures 5 and 6 show the VACs of the specimens with Cr and ITO electrodes after different annealing duration.

One can note the following specific features of these VACs:

– the VACs are nonlinear near zero for the specimens with ITO electrodes;

– the difference between the measurement cycles in the VACs for the specimens with ITO electrodes decreases and VAC nonlinearity near $U = 0$ also decreases with an increase in annealing duration;

– VAC nonlinearity near $U = 0$ for the specimens with Cr electrodes is noticeably lower than that for the specimens with ITO electrodes.

The VACs of some specimens exhibit hysteresis loops attributable to relaxation processes. To study the relaxation processes we analyzed current *vs* time curves at a constant voltage for all the specimens. The results showed that for an absolute voltage value of above 5 V the decrease of current in time for all the specimens is within 2% of the maximum values. Furthermore for VAC measurements in the –5 to 5 V range, VAC nonlinearity significantly affects the electrical conductivity readings. At higher voltages the nonlinearity has a smaller effect on the electrical conductivity measurement results. Therefore when measuring the electrical conductivity we did not use the current readings taken in the –5 to 5 V range. The resistivities were calculated for each measurement cycle separately for the positive and negative VAC branches.

The asymmetrical pattern of the curves for the specimens with chromium electrodes shown in Figs. 5 and 6 is far less expressed than for the specimens with ITO electrodes. The VACs of the specimens with ITO electrodes exhibit a low-conductivity section covering a range of approx. 2 V (Fig. 6 *b*). These features can be caused by the presence of an energy barrier at the interface between reduced lithium niobate and the electrode material or by charging of the intrinsic capacity and polarization currents [18]. However, in earlier studies of current relaxation phenomena in polar crystalline dielectrics [21–24] the relaxation was attributed to galvanic interaction of the

electrode material with the specimen material at room temperature which also causes emf.

3.2. Impedance measurements

Impedance spectroscopy data are shown in the form of Nyquist hodograph diagrams in Fig. 7.

It can be seen from Fig. 7 that all the hodograph diagrams calculated within the simplest model shown in Fig. 4 *a* (Fig. 7, Curves *3*) contradict with the experimental data (Curve *1*). This fact suggests that the experimental room temperature electrical conductivities of reduced lithium niobate are significantly affected by the non-ohmicity of the contacts. The discrepancy between the measured and theoretical data in the Nyquist hodograph diagrams can be accounted for by the presence of potential barriers at the interface between the specimen and the electrode (depleted layers) or by the relatively

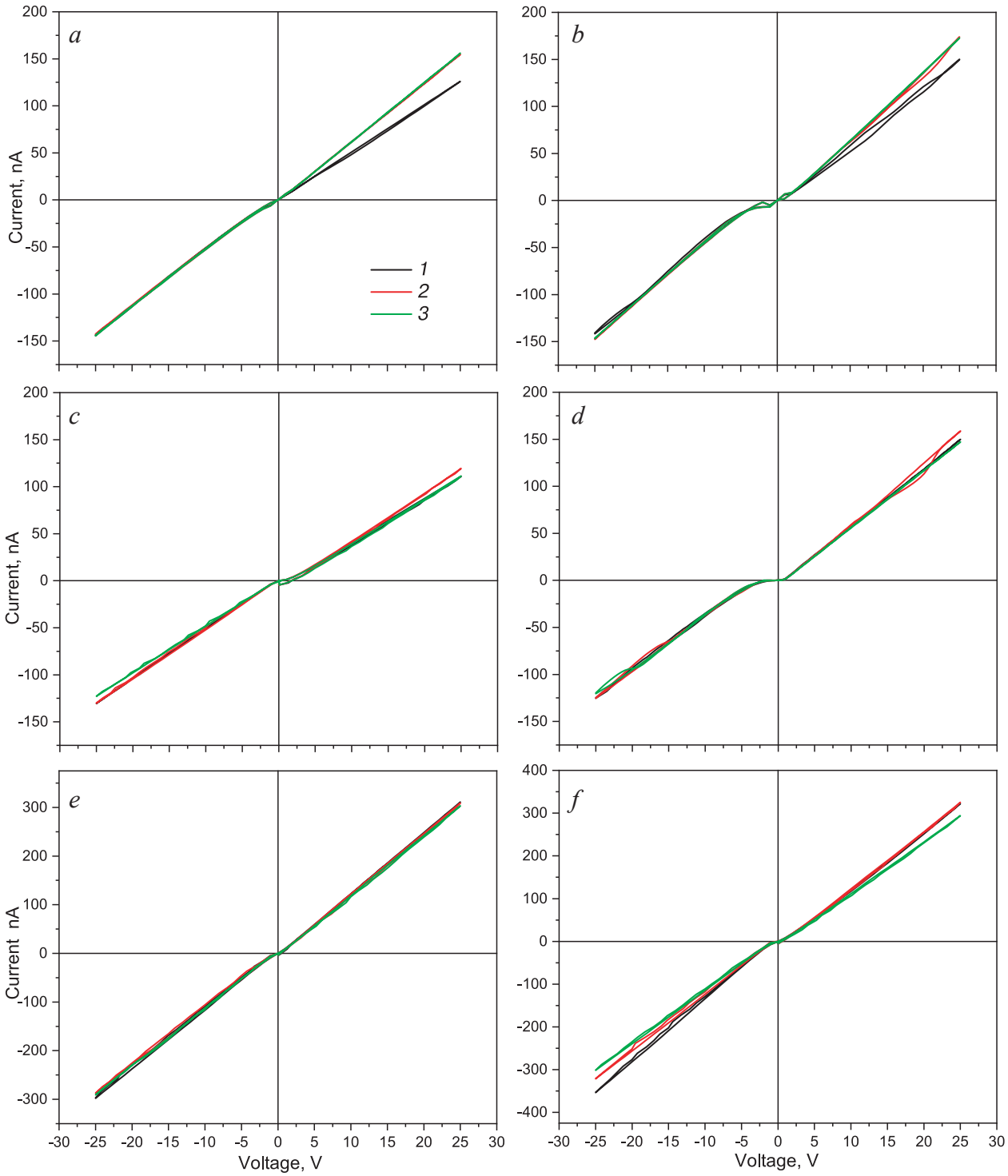

Figure 5. VACs for specimens with (*a*, *c* and *e*) Cr and (*b*, *d* and *f*) ITO electrodes as-annealed for (*a* and *b*) 2, (*c* and *d*) 20 and (*e* and *f*) 40 min. taken in the –25 to 25 V range: (*1*, *2* and *3*) are the first, second and third measurement cycles.

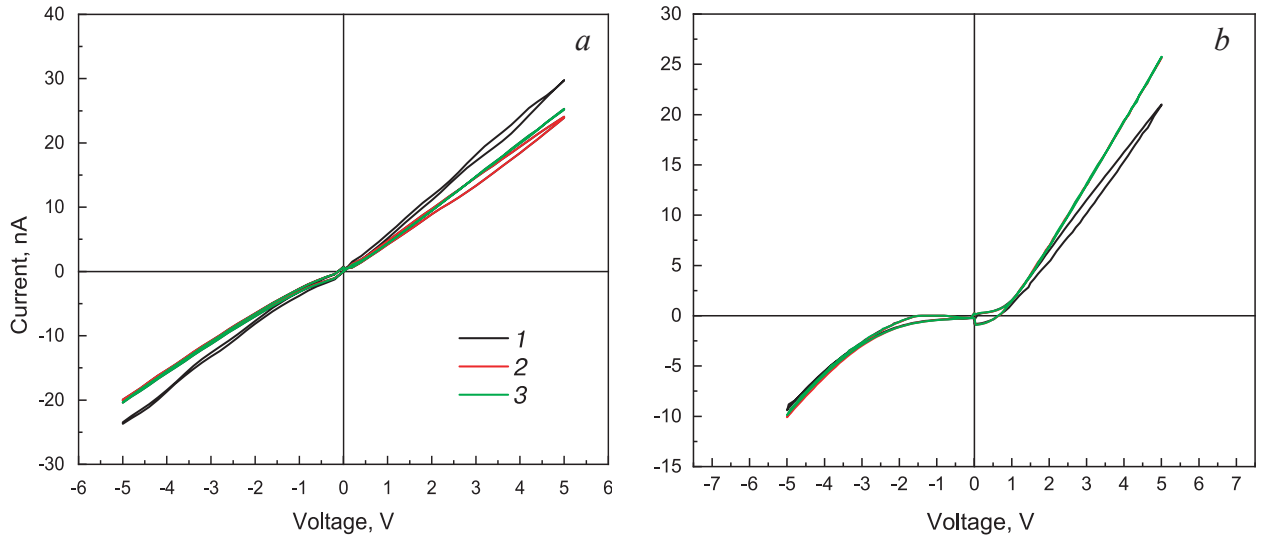

Figure 6. VAC for specimens with (*a*) Cr and (*b*) ITO electrodes as-annealed for 2 min. taken in the –5 to 5 V range: (*1*, *2* and *3*) are the first, second and third measurement cycles.

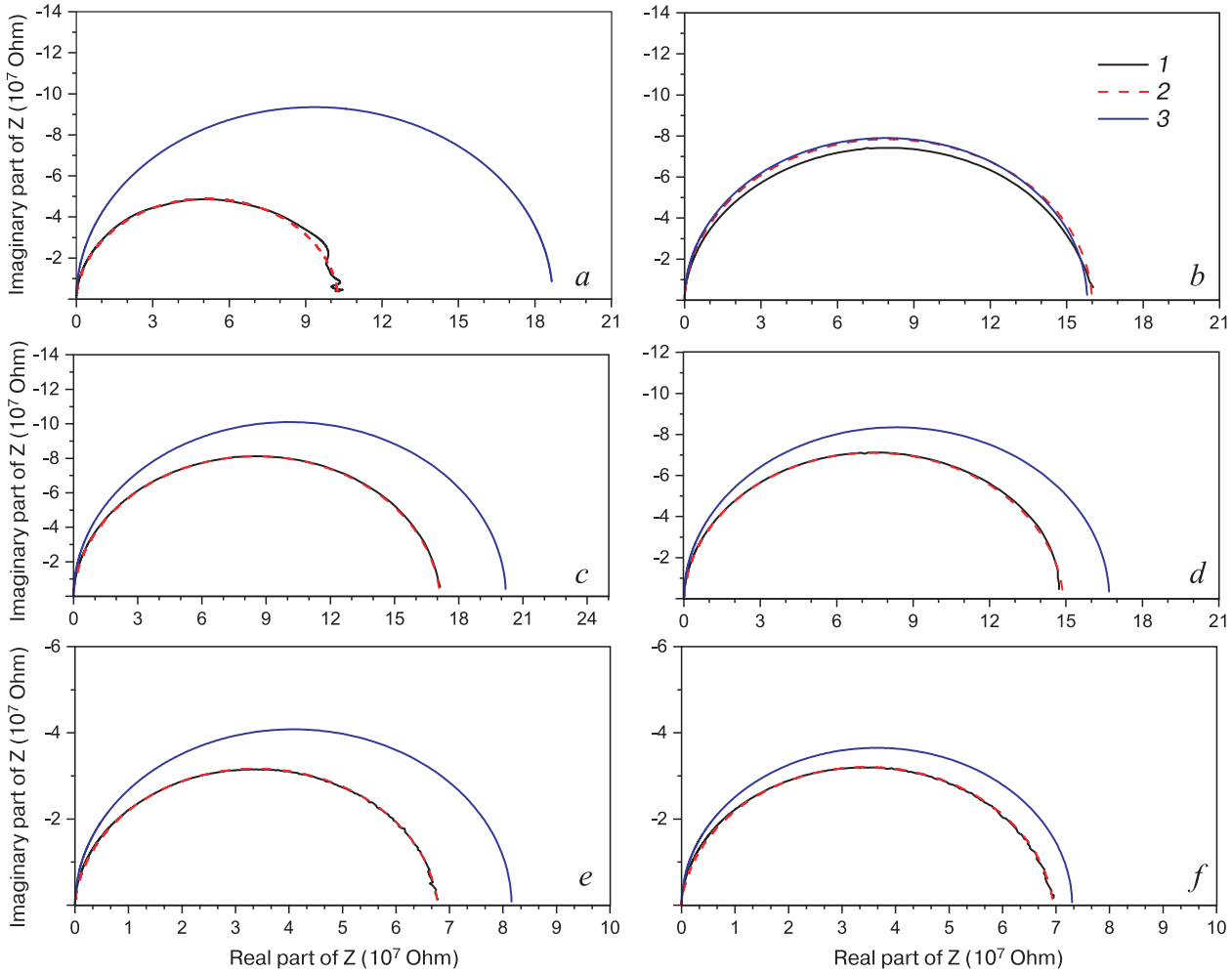

Figure 7. Nyquist hodograph diagrams of impedance spectra for specimens with (*a*, *c* and *e*) Cr and (*b*, *d* and *f*) ITO electrodes as-annealed for (*a* and *b*) 2, (*c* and *d*) 20 and (*e* and *f*) 40 min.: (*1*) experimental curve and (*2* and *3*) calculation on the basis of equivalent circuits shown in Fig. 4 *b* and 4 *a*, respectively.

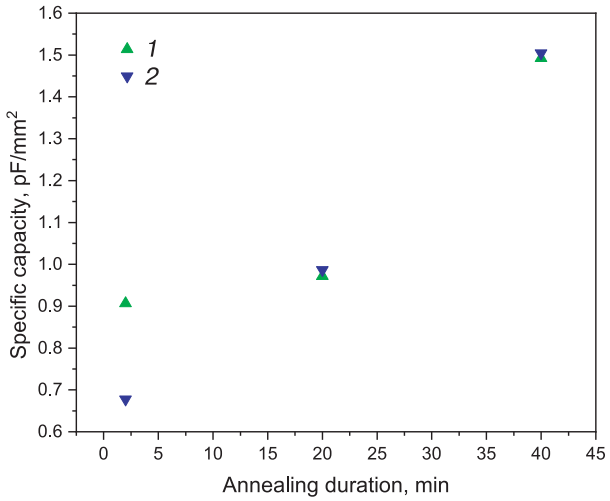

Figure 8. Specific capacity as a function of annealing duration for specimens with (*1*) Cr and (*2*) ITO electrodes.

high density of electron states (electron traps). To verify this hypothesis we analyzed the dependence of the electrical capacity of the specimens at 1 kHz (Fig. 8) on annealing duration.

Since reduction annealing does not cause lithium niobate transformation to a new phase with a higher dielectric permeability, the electrical capacity of the specimen cannot change significantly due to a change in the dielectric parameters.

However Fig. 8 well illustrates the growth of the specific capacity. This phenomenon originates from the additional capacity at the electrode / lithium niobate interface. There are two possible variants:

– a depleted layer forming near the contact;

– change of charge of the electron states at the contact/specimen interface upon application of an AC bias during the measurements.

In the former case the capacities are connected in series and in the latter case they are parallel. For serial connection the resultant capacity C_{res} cannot exceed the capacity of the specimen C_{spc} at any contact barrier capacity C_{bar}:

$$C_{res} = \frac{C_{spc}C_{bar}}{C_{spc} - C_{bar}}.$$

Since the results suggest that $C_{res} \geq C_{spc}$, one can state that the capacity of the specimen and the contact capacity are parallel. The experiments also suggest that the resultant capacity is as follows:

$$C_{res} = C_{spc} + C_{bar},$$

where $C_{spc} = const$ increases in with an increase in annealing duration and carrier concentration, this being in agreement with the observed increase in the electrical conductivity of the specimens. We therefore approximated the experimental data with the equivalent circuit as shown in Fig. 4 *b*. The results of experimental data approximation using Eq. (1) are shown in Fig. 7, Curve *2*.

Selected parameters of equivalent circuit components providing for the best fit with the experimental curves with normalization to the specimen dimensions are shown in the form of specific electrical resistivity (the R and R_{VAC} elements of the equivalent electric circuit in Fig. 4) as a function of annealing duration (Fig. 9) and the *CPE* parameter as a function of annealing duration (Fig. 10). The exponent n in Eq. (1) takes on 0.87 for the specimens with chromium electrodes annealed for 2 and 20 min. and $n = 0.9$ for the other as-annealed specimens. These exponential value suggest that the performance parameters of the *CPE* elements shown in the hodograph diagrams are close to those of capacitors and the *CPE* element itself is in this case referred to as the fractal capacitor [24]. Furthermore the exponents n do not fit into the range of (0.25–0.75) in which the *CPE* element degrades to a Warburg diffusion element [24]. This suggests the absence of any significant diffusion processes in the near-electrode regions and in the specimen bulk.

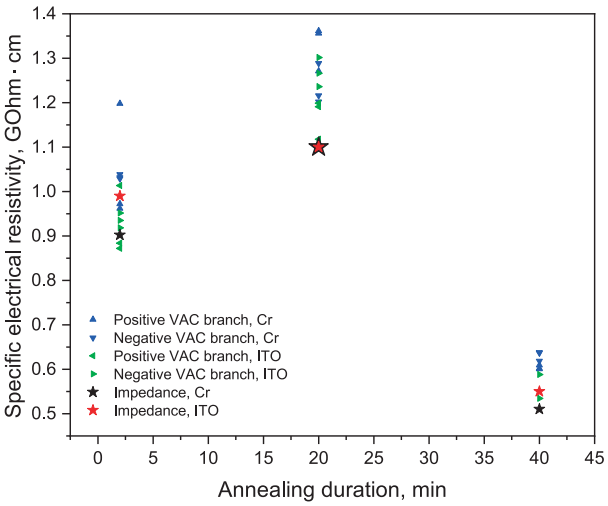

Figure 9. Specific electrical resistivity as a function of annealing duration for specimens with chromium and ITO electrodes, as per measurements of positive and negative VAC branches (triangles) and impedance spectra.

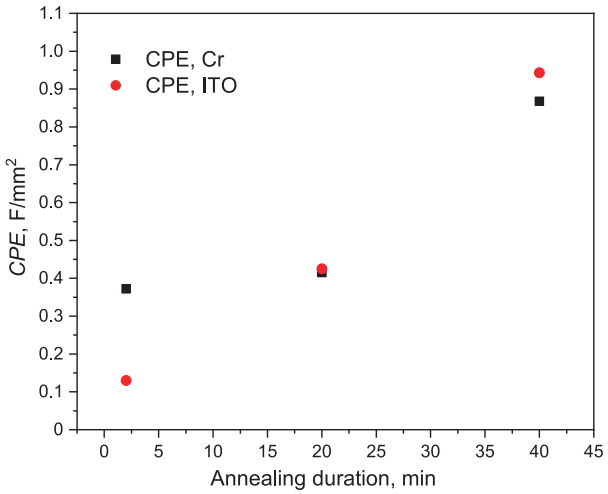

Figure 10. CPE of reduced specimens as a function of annealing duration.

The data shown in Fig. 9 suggest that the specific resistivity of the specimens is a nonmonotonic function of annealing duration. Similar results were obtained earlier [8] in a study of room temperature electrical resistivity as a function of annealing temperature for constant exposure time. The data suggest that the conductivity *vs* annealing temperature is a nonmonotonic function with a minimum for specimens annealed at 1000 °C. The authors explained this behavior within a polaron conductivity model, i.e., the conductivity increases due to the Nb_{Nb}^{5+} to Nb_{Li}^{4+} transitions, with the maximum value occurring at some critical ratio of Nb_{Nb}^{5+} and Nb_{Li}^{4+}. Further reduction annealing leads to a decrease in the quantity of polarons due to the destruction of bipolarons resulting in a decrease in the concentration of mobile carriers and hence a decrease in the electrical conductivity. The above line of reasoning is also true for the dependences of room temperature electrical conductivity on constant-temperature annealing duration since in that case the formation of polarons occurs by the same mechanism.

The growth of the fractal capacity with an increase in annealing duration (see Fig. 8) is probably caused by the fact that an increase in the concentration of mobile carriers (polarons) entails a higher occupation of electron states at the specimen/contact interface. One should also take into account a possible increase in the density of states during high-temperature anneals.

4. Conclusion

Reduction vacuum annealing of lithium niobate at 1050 °C reduces the electrical resistivity of the material, however the dependence on annealing duration is nonmonotonic: crystal exposure to an oxygen-free atmosphere for 40 min causes a drop in the electrical resistivity to $5 \cdot 10^8$ Ohm · cm. The measurement results depend significantly on the electrode material, especially at low voltages.

Chromium electrodes form close-to-Ohmic contacts to reduced lithium niobate crystals but for short annealing duration in an oxygen-free atmosphere (20 min or less) the VACs are nonlinear close to zero voltage. The VACs for ITO electrodes contacting with lithium niobate have a clearly manifested nonlinear pattern with a reduction in the nonlinearity for long exposure (40 min) but without complete nonlinearity elimination.

We showed that with an increase in annealing duration the capacity of the specimens with both chromium and ITO electrodes increases. Our hypothesis is that this phenomenon is attributed to charge accumulation at electron states at the specimen / contact material interface. We suggested and calculated an equivalent circuit in which the contact capacity is represented as a fractal capacitor.

Acknowledgments

The study was conducted with financial support from the Russian Research Foundation (Grant No. 21-19-00872, https://rscf.ru/project/21-19-00872/) for specimen preparation and reduced lithium niobate electrophysical measurements.

The Authors are grateful to the Ministry of Education and Science of the Russian Federation for support within State Assignment (Fundamental Research Project No. 0718-2020-0031 “New Ferroelectric Composite Materials on the Basis of Oxide Ferroelectrics with Ordered Domain Structure: Production and Properties”).

Impedance spectroscopic studies were carried out on equipment of the Collective Use Center “Materials Science and Metallurgy” of the MISiS National Research and Technology University with financial support from the Ministry of Education and Science of the Russian Federation (No. 075-15-2021-696).

References

1. Kubasov I.V., Kislyuk A.M., Turutin A.V., Bykov A.S., Kiselev D.A., Temirov A.A., Zhukov R.N., Sobolev N.A., Malinkovich M.D., Parkhomenko Y.N. Low-frequency vibration sensor with a sub-nm sensitivity using a bidomain lithium niobate crystal. *Sensors (Basel)*. 2019; 19(3): 614. https://doi.org/10.3390/s19030614
2. Turutin A.V., Vidal J.V., Kubasov I.V., Kislyuk A.M., Malinkovich M.D., Parkhomenko Y.N., Kobeleva S.P., Pakhomov O.V., Kholkin A.L., Sobolev N.A. Magnetoelectric metglas/bidomain y + 140°-cut lithium niobate composite for sensing fT magnetic fields. Appl. Kubasov I.V, Kislyuk A.M., Turutin A.V, Malinkovich M.D., Parkhomenko Y.N. Bidomain Ferroelectric Crystals: Properties and Prospects of Application. *Phys. Lett*. 2018; 112(26): 262906. https://doi.org/10.1063/1.5038014
3. Kubasov I.V., Kislyuk A.M., Ilina T.S., Shportenko A.S., Kiselev D.A., Turutin A.V., Temirov A.A., Malinkovich M.D., Parkhomenko Y.N. Conductivity and memristive behavior of completely charged domain walls in reduced bidomain lithium niobate. *J. Mater. Chem. C*. 2021; 9(43). https://doi.org/10.1039/d1tc04170C
4. Kubasov I.V., Kislyuk A.M., Turutin A.V., Malinkovich M.D., Parkhomenko Yu.N. Bidomain ferroelectric crystals: properties and prospects of application. *Izvestiya Vysshikh Uchebnykh Zavedenii. Materialy Elektronnoi Tekhniki = Materials of Electronics Engineering*. 2020; 23(1): 5–56. (In Russ.). https://doi.org/10.17073/1609-3577-2020-1-5-56
5. Standifer E.M., Jundt D.H., Norwood R.G., Bordui P.F. Chemically reduced lithium niobate single crystals: processing, properties and improvements in SAW device fabrication and performance. In: *Proc. IEEE International Frequency Control Symposium*. 1998: 470–472. https://doi.org/10.1109/FREQ.1998.717939

6. Jen S., Bobkowski R. Black lithium niobate SAW device fabrication and performance evaluation. In: *Proc. IEEE Ultrasonics Symposium*. 2000: 269–273. https://doi.org/10.1109/ultsym.2000.922554
7. Kuzminov Yu.S. Electro-optical and nonlinear-optical lithium niobate crystal: monograph. Moscow: Nauka; 1987: 264 p. (In Russ.)
8. Palatnikov M.N., Sandler V.A., Sidorov N.V., Makarova O.V., Manukovskaya D.V. Conditions of application of $LiNbO_3$ based piezoelectric resonators at high temperatures. *Phys. Lett. A*. 2020; 384(14): 126289. https://doi.org/10.1016/j.physleta.2020.126289
9. Yatsenko A.V., Pritulenko A.S., Yagupov S.V., Sugak D.Y., Sol'skii I.M. Investigation of the stability of electrical properties of reduced $LiNbO_3$ crystals. *Tech. Phys*. 2017; 62(7): 1065–1068. https://doi.org/10.1134/s1063784217070271
10. Dhar A., Singh N., Singh R.K., Singh R. Low temperature dc electrical conduction in reduced lithium niobate single crystals. *J. Phys. Chem. Solids*. 2013; 74(1): 146–151. https://doi.org/10.1016/j.jpcs.2012.08.011
11. Volk T., Wöhlecke M. Lithium niobate: defects, photorefraction and ferroelectric switching. Berlin: Springer Science & Business Media; 2008: 249 p.
12. Singh K. Electrical conductivity of non-stoichiometric $LiNbO_3$ single crystals. *Ferroelectrics*. 2004; 306(1): 79–92. https://doi.org/10.1080/00150190490457348
13. Yatsenko A.V., Yevdokimov S.V., Pritulenko A.S., Sugak D.Y., Solskii I.M. Electrical properties of $LiNbO_3$ crystals reduced in a hydrogen atmosphere. *Phys. Solid State*. 2012; 54(11): 2231–2235. https://doi.org/10.1134/S1063783412110339
14. Bordui P.F., Jundt D.H., Standifer E.M., Norwood R.G., Sawin R.L., Galipeau J.D. Chemically reduced lithium niobate single crystals: Processing, properties and improved surface acoustic wave device fabrication and performance. *J. Appl. Phys*. 1999; 85(7): 3766–3769. https://doi.org/10.1063/1.369775
15. Yatsenko A.V., Pritulenko A.S., Yevdokimov S.V., Sugak D.Y., Syvorotka I.I., Suhak Y.D., Solskii I.M., Vakiv M.M. The influence of annealing in saturated water vapor on $LiNbO_3$ crystals optical and electrical properties. *Solid State Phenomena*. 2015; 230: 233–237. https://doi.org/10.4028/www.scientific.net/SSP.230.233
16. Akhmadullin I.Sh., Golenishchev-Kutuzov V.A., Migachev S.A., Mironov S.P. Low-temperature electrical conductivity of lithium niobate crystals of congruent composition. *Fizika tverdogo tela*. 1998; 40(7): 1307–1309. (In Russ.)
17. Schröder M., Haußmann A., Thiessen A., Soergel E., Woike T., Eng L.M. Conducting domain walls in lithium niobate single crystals. *Adv. Funct. Mater*. 2012; 22(18): 3936–3944. https://doi.org/10.1002/adfm.201201174
18. Sanna S., Schmidt W.G. $LiNbO_3$ surfaces from a microscopic perspective. *J. Phys.: Condens. Matter.* 2017; 29(41): 413001. https://doi.org/10.1088/1361-648X/aa818d
19. Esin A.A., Akhmatkhanov A.R., Shur V.Y. The electronic conductivity in single crystals of lithium niobate and lithium tantalate family. *Ferroelectrics*. 2016; 496(1): 102–109. https://doi.org/10.1080/00150193.2016.1157438
20. Wang C., Sun J., Ni W., Yue B., Hong F., Liu H., Cheng Z. Tuning oxygen vacancy in $LiNbO_3$ single crystals for prominent memristive and dielectric behaviors. *J. Am. Ceram. Soc*. 2019; 102(11): 6705–6712. https://doi.org/10.1111/jace.16522
21. Blistanov A.A., Kozlova N.S., Geras'kin V.V. The phenomenon of electrochemical self-decomposition in polar dielectrics. *Ferroelectrics*. 1997; 198(1-4): 61–66. https://doi.org/10.1080/00150199708228338
22. Kozlova N.S., Zabelina E.V., Bykova M.B., Kozlova A.P. Features of manifestation of surface electrochemical processes in ferroelectric crystals with low-temperature phase transitions. *Izvestiya Vysshikh Uchebnykh Zavedenii. Materialy Elektronnoi Tekhniki = Materials of Electronics Engineering*. 2018; 21(3): 146–155. (In Russ.). https://doi.org/10.17073/1609-3577-2018-3-146-155
23. Buzanov O.A., Zabelina E.V., Kozlova N.S., Sagalova T.B. Near-electrode processes in lanthanum-gallium tantalate crystals. *Crystallogr. Rep*. 2008; 53(5): 853–857. https://doi.org/10.1134/S1063774508050210
24. Kozlova N.S., Zabelina E.V., Bykova M.B., Kozlova A.P. Features of the manifestation of surface electrochemical processes in ferroelectric crystals with low-temperature phase transitions. *Russ. Microelectron.* 2019; 48(8): 545–552. https://doi.org/10.1134/S1063739719080092
25. Emelyanova Yu.V., Morozova M.V., Mikhailovskaya Z.A., Buyanova E.S. Impedance spectroscopy: theory and application: textbook. allowance. Yekaterinburg: Ural Federal University named after the first President of Russia B.N. Yeltsin; 2017: 156 p. (In Russ.)